ISSN 1674-1056
http://cpb.iphy.ac.cn
http://iopscience.iop.org/cpb
中国物理 B
Chinese Physics
中国物理 Chinese Physics B

Multi-bubble motion behavior of uniform magnetic field based on phase field model

Chang-Sheng Zhu(朱昶胜), Zhen Hu(胡震), Kai-Ming Wang(王凯明)

Citation: Chin. Phys. B . 2020, 29(3): 034702 . **doi:** 10.1088/1674-1056/ab6839
Journal homepage: http://cpb.iphy.ac.cn; http://iopscience.iop.org/cpb

What follows is a list of articles you may be interested in

Numerical simulation on dynamic behaviors of bubbles flowing through bifurcate T-junction in microfluidic device

Liang-Yu Wu(吴梁玉), Ling-Bo Liu(刘凌波), Xiao-Tian Han(韩笑天), Qian-Wen Li(李倩文), Wei-Bo Yang(杨卫波)
Chin. Phys. B . 2019, 28(10): 104702 . **doi:** 10.1088/1674-1056/ab3f27

Direct numerical simulation on relevance of fluctuating velocities and drag reduction in turbulent channel flow with spanwise space-dependent electromagnetic force

Dai-Wen Jiang(江代文), Hui Zhang(张辉), Bao-Chun Fan(范宝春), An-Hua Wang(王安华)
Chin. Phys. B . 2019, 28(5): 054701 . **doi:** 10.1088/1674-1056/28/5/054701

Phase field simulation of single bubble behavior under an electric field

Chang-Sheng Zhu(朱昶胜), Dan Han(韩丹), Sheng Xu(徐升)
Chin. Phys. B . 2018, 27(9): 094704 . **doi:** 10.1088/1674-1056/27/9/094704

A new kind of hairpin-like vortical structure induced by cross-interaction of sinuous streaks in turbulent channel

Jian Li(李健), Gang Dong(董刚), Hui Zhang(张辉), Zhengshou Chen(陈正寿), Zhaode Zhang(张兆德)
Chin. Phys. B . 2018, 27(8): 084701 . **doi:** 10.1088/1674-1056/27/8/084701

Mechanism of controlling turbulent channel flow with the effect of spanwise Lorentz force distribution

Yang Han(韩洋), Hui Zhang(张辉), Bao-Chun Fan(范宝春), Jian Li(李健), Dai-Wen Jiang(江代文), Zi-Jie Zhao(赵子杰)
Chin. Phys. B . 2017, 26(8): 084704 . **doi:** 10.1088/1674-1056/26/8/084704

Multi-bubble motion behavior of uniform magnetic field based on phase field model*

Chang-Sheng Zhu(朱昶胜)[1,2,†], Zhen Hu(胡震)[1], and Kai-Ming Wang(王凯明)[1]

[1] School of Computer and Communication, Lanzhou University of Technology, Lanzhou 730050, China
[2] State Key Laboratory of Gansu Advanced Processing and Recycling of Non-Ferrous Metal, Lanzhou University of Technology, Lanzhou 730050, China

(Received 23 September 2019; revised manuscript received 14 November 2019; accepted manuscript online 7 January 2020)

Aiming at the interaction and coalescence of bubbles in gas–liquid two-phase flow, a multi-field coupling model was established to simulate deformation and dynamics of multi-bubble in gas–liquid two-phase flow by coupling magnetic field, phase field, continuity equation, and momentum equation. Using the phase field method to capture the interface of two phases, the geometric deformation and dynamics of a pair of coaxial vertical rising bubbles under the applied uniform magnetic field in the vertical direction were investigated. The correctness of results is verified by mass conservation method and the comparison of the existing results. The results show that the applied uniform magnetic field can effectively shorten the distance between the leading bubble and the trailing bubble, the time of bubbles coalescence, and increase the velocity of bubbles coalescence. Within a certain range, as the intensity of the applied uniform magnetic field increases, the velocity of bubbles coalescence is proportional to the intensity of the magnetic field, and the time of bubbles coalescence is inversely proportional to the intensity of the magnetic field.

Keywords: bubbles coalescence, uniform magnetic field, numerical simulation, phase field method

PACS: 47.11.–j, 47.55.dd **DOI:** 10.1088/1674-1056/ab6839

1. Introduction

Gas–liquid two-phase flow with bubbles as the dispersed phase is common in many industrial applications, such as material research, metallurgical engineering, electrolytic machining, petrochemical industry, chemical engineering, energy power, nuclear fusion reaction, and so on.[1–3] The interaction and coalescence of bubbles in liquid will have a significant impact on the gas–liquid contact time and contact area, which indirectly changes the heat transfer, mass transfer, and chemical reaction in the gas–liquid system. Therefore, research on gas–liquid two-phase flow is of great value.

Due to the complexity of gas–liquid two-phase flow, more and more researches on the motion of gas–liquid two-phase flow have started to use numerical simulation in recent years. Firstly, it can reduce the time and cost of the experiment; secondly, it can reduce the risk of the experimenters in the dangerous experimental environment; thirdly, it can discover some important information that cannot be obtained in the experiment. The numerical simulation of free-interface deformation in gas–liquid two-phase flow is very complicated, and there are many numerical simulation methods. The phase field method[4] considers that the interface is a smooth transition region with a certain width, a phase variable is introduced in the flow field. The phase variable is constant inside the single-medium fluid and continuously changes in the interface region. The interface of multiple media is represented by a contour line (contour surface) of the phase variable. The motion of the interface is controlled by updating the fourth-order partial differential Cahn–Hilliard (CH) equation of the phase variable. The phase field method can deal with multi-media problems with complex geometric topology changes on the interface, including complex structural changes such as splitting and fusion of interfaces. The phase field method does not require a reinitialization step in the level set method, nor does it require a reconfiguration of interface in the volume-of-fluid (VOF) method. It greatly reduces the amount of computation, from the programming point of view, it is easier to implement and promote to high-dimensional problems. The interface information functions in the VOF and level-set methods are the volume ratio of the fluid independent of the flow parameters and the signed distance function of the interface, respectively. The phase variables in the phase field method are the physical quantities associated with the flow parameters. In this case, the CH equation can be solved by coupling with the flow control equation, thereby avoiding the destruction of the physical conservation relationship caused by artificial processing near the interface. The phase field calculation method can effectively simulate the gas–liquid two-phase flow problem with large-density ratio by coupling the phase field with other external fields such as gravity field, flow field, temperature field, electric field, and magnetic field.

The applied magnetic field is one of the effective methods to control the change of bubbles in the gas–liquid two-phase

*Project supported by the National Natural Science Foundation of China (Grant Nos. 51661020, 11504149, and 11364024), the Postdoctoral Science Foundation of China (Grant No. 2014M560371), and the Funds for Distinguished Young Scientists of Lanzhou University of Technology (Grant No. J201304).

†Corresponding author. E-mail: zhucs2008@163.com

© 2020 Chinese Physical Society and IOP Publishing Ltd

flow without contact. Nakatsuka *et al.*[5] considered the magnetic field effects of air and steam bubbles in a non-uniform magnetic field in the experiment and found that the applied magnetic field can control the flow of bubbles in the heat pipe and increase the heat transfer rate. Tagawa[6] conducted a research on the effects of a non-uniform magnetic field on a dielectric fluid, using the electrolytic potential solution method to calculate the Lorentz force. In his research, Ki[7] numerically simulates the effects of an applied uniform magnetic field on dielectric single bubbles and droplets. Sihafiei Dizaji *et al.*[8] numerically simulated the dynamics of steam bubbles rising in ferrofluid in the presence of a magnetic field by using the VOF method. Ansari *et al.*[9] also studied the dynamics of a single bubble in a liquid column with the level-set method, where both phases are dielectric. Guo *et al.*[10] coupled the VOF and level-set methods to study the MNF (magnetic mean nanofluid) film under the effects of uniform magnetic field. In her research, Tian[11] used the VOF method to study the motion behavior of multiple bubbles in conductive fluid under the effects of uniform vertical magnetic field. Numerical simulation of bubbles coalescence in media under the effects of uniform magnetic field by Hadidi *et al.*[12] These researchers found that a uniform magnetic field only affects the interface of bubbles in the dielectric field. Phase field method is one of the most popular interface capture methods for simulating complex incompressible multi-media, but it is rarely used in previous experimental studies. Therefore, the phase field method is used to numerically simulate the deformation and dynamic behavior of a pair of bubbles coalescing in a vertical uniform magnetic field.

2. Mathematical model

2.1. Governing equations

Yue *et al.*[13] proposed a famous continuity equation and momentum equation for the phase field simulation of two-phase systems of microstructured complex fluids. But the two equations are obviously different from the continuity equation and momentum equation of this study. In this study, considering that both phases of gas–liquid two-phase flow are inmiscible and viscous incompressible fluids, and under the effects of gravity, surface tension, and magnetic field forces, the continuity equation and momentum equation[14] are expressed as follows:

$$\nabla \cdot \boldsymbol{u} = 0, \tag{1}$$

$$\begin{aligned} &\frac{\partial(p(\phi)\boldsymbol{u})}{\partial t} + \rho(\phi)\boldsymbol{u}\cdot\nabla\boldsymbol{u} + \nabla p \\ &= \nabla\cdot[\mu(\phi)(\nabla\boldsymbol{u} + \nabla\boldsymbol{u}^{\mathrm{T}})] + \rho(\phi)\boldsymbol{g} + \boldsymbol{F}_{\mathrm{st}} + \boldsymbol{F}_{\mathrm{mf}}, \end{aligned} \tag{2}$$

where $\boldsymbol{u}$ is the velocity vector of the fluid, $\rho(\phi)$ is the density of the fluid, t is the time, p is the pressure, $\mu(\phi)$ is the dynamic viscosity coefficient, $\rho(\phi)\boldsymbol{g}$ is the gravity, $\boldsymbol{F}_{\mathrm{st}}$ is the source of the surface tension, $\boldsymbol{F}_{\mathrm{mf}}$ is the magnetic field force ϕ is a dimensionless phase field variable,[15]

$$\phi(x,t) = \begin{cases} 1, & \text{fluid 1,} \\ -1 \leqslant x \leqslant 1, & \text{interfacial transition region,} \\ -1, & \text{fluid 2.} \end{cases} \tag{3}$$

2.2. Phase field equation

Complex motion changes and geometric topological changes occur during the coalescence of bubbles in a gas–liquid two-phase flow. Therefore, the key to this research is to be able to capture the changes of the interface. The phase field method tracks the change of the interface by updating the fourth-order partial differential CH equation of the phase variable,[16,17]

$$\frac{\partial\phi}{\partial t} + \boldsymbol{u}\cdot\nabla\phi = \nabla\cdot\frac{\gamma\lambda}{\xi^2}\nabla\varphi = \nabla\cdot\gamma\nabla G, \tag{4}$$

$$\varphi = -\nabla\cdot\xi^2\nabla\phi + (\phi^2-1)\phi. \tag{5}$$

In Eqs. (4) and (5), the symbol ϕ is an auxiliary variable of the phase field.

G is the chemical potential, and its expression is

$$G = \frac{\delta F}{\delta\phi} = \lambda\left[-\nabla^2\phi + \frac{(\phi^2-1)\phi}{\xi^2}\right], \tag{6}$$

where ξ is the interface thickness control parameter, σ is the surface tension coefficient, and λ is the mixed energy density. They satisfy the following equation:

$$\lambda = \frac{3\xi\sigma}{\sqrt{8}}. \tag{7}$$

Based on Eq. (7), the free energy[13] F can be expressed as

$$F = \int [f']\mathrm{d}\Omega = \int\left[\frac{\lambda}{2}|\nabla\phi|^2 + f\right]\mathrm{d}\Omega, \tag{8}$$

where f' is the free energy density, and f is bulk energy, and its expression is

$$f = \frac{\lambda}{4\xi^2}(\phi-1)^2(\phi+1)^2. \tag{9}$$

The mobility, γ, is described by ξ and the migration adjustment parameter χ, where χ is taken as 1 in this experimental study,

$$\gamma = \chi\xi^2. \tag{10}$$

2.3. Surface tension formula

In the phase field method, the interface is considered to be a continuous transition region of a certain width, so that the surface tension is continuously distributed in the transition region, which can be expressed by the following equation:

$$\boldsymbol{F}_{\mathrm{st}} = G\nabla\phi. \tag{11}$$

$\boldsymbol{F}_{\mathrm{st}}$ is used to solve the gas–liquid two-phase flow by adding the Navi–Stokes (NS) equation as a volume force.

2.4. Magnetic field

The magnetic force acts only on the interface where the magnetic permeability is discontinuous, and it will disappear if the magnetic permeability is constant. The magnetic field applied to the flow field area will exert an inducing force at the interface of the two phases, which can be expressed as

$$\boldsymbol{F}_{\mathrm{mf}} = \nabla\cdot(\eta_0\eta(\phi)\boldsymbol{H}\boldsymbol{H}) - \frac{1}{2}\boldsymbol{H}^2\nabla\eta_0\eta(\phi) + \nabla\left(\frac{1}{2}\rho\frac{\partial\eta_0\eta(\phi)}{\partial\rho}\boldsymbol{H}^2\right), \tag{12}$$

where η_0 is the vacuum permeability, $\eta(\phi)$ is the relative permeability of the medium, ρ is the density of the medium, $\boldsymbol{H}$ is the magnetic field intensity which can be described by equation of $\boldsymbol{H} = -\nabla\psi$, and ψ is the magnetic scalar potential.[18] The third term in Eq. (12) is used to characterize the magnetostriction phenomenon. Considering that the two-phase fluid is incompressible, the third term can be ignored,[19] so the final magnetic field force can be expressed as

$$\boldsymbol{F}_{\mathrm{mf}} = \nabla\cdot(\eta_0\eta(\phi)\boldsymbol{H}\boldsymbol{H}) - \frac{1}{2}\boldsymbol{H}^2\nabla\eta_0\eta(\phi). \tag{13}$$

In the absence of an electric field, the four equations in Maxwell's equations are reduced to the following two equations:

$$\nabla\cdot\boldsymbol{B} = 0, \tag{14}$$

$$\nabla\times\boldsymbol{H} = \boldsymbol{J}_{\mathrm{c}}, \tag{15}$$

$$\boldsymbol{B} = \eta(\phi)\boldsymbol{H}, \tag{16}$$

where $\boldsymbol{B}$ is the magnetic field applied to the fluid, and $\boldsymbol{J}_{\mathrm{c}}$ is the electric current. Considering that there is no applied current in this study, $\boldsymbol{J}_{\mathrm{c}} = 0$. Therefore, the equation satisfying Eqs. (14) and (15) can be obtained as

$$\nabla\cdot(\eta(\phi)\psi) = 0. \tag{17}$$

2.5. Fluid property parameters

In this study, the relevant fluid property parameters are as follows:

$$\rho(\phi) = \frac{1+\phi}{2}\rho_{\mathrm{g}} + \frac{1-\phi}{2}\rho_{\mathrm{l}}, \tag{18}$$

$$\mu(\phi) = \frac{1+\phi}{2}\mu_{\mathrm{g}} + \frac{1-\phi}{2}\mu_{\mathrm{l}}, \tag{19}$$

$$\eta(\phi) = \frac{1+\phi}{2}\eta_{\mathrm{g}} + \frac{1-\phi}{2}\eta_{\mathrm{l}}, \tag{20}$$

where the subscripts "g" and "l" represents the gas and liquid phases, respectively.

2.6. Dimensionless parameters

The dimensionless parameters, including the Eotvos number Eo, the Morton number Mo,[20] the Reynolds number Re, and the Weber number We, are used to describe the motion characteristics of the bubble, which are calculated as follows:

$$Eo = \frac{\boldsymbol{g}(\rho_{\mathrm{l}}-\rho_{\mathrm{g}})d^2}{\sigma}, \tag{21}$$

$$Mo = \frac{\boldsymbol{g}(\rho_{\mathrm{l}}-\rho_{\mathrm{g}})\mu_{\mathrm{l}}^4}{\rho_{\mathrm{l}}^2\sigma^3}, \tag{22}$$

$$Re = \frac{\rho_{\mathrm{l}}ud}{\mu_{\mathrm{l}}}, \tag{23}$$

$$We = \frac{g\mu_{\mathrm{l}}^4}{\rho_{\mathrm{l}}\sigma^3}, \tag{24}$$

where $\boldsymbol{g}$ is the gravitational acceleration, d is the bubble diameter, Eo is the ratio of the buoyancy to the surface tension, and Mo is the characteristic of the external fluid. These two numbers are controllable. Re and We describe the bubble rise rate and bubble characteristics, respectively. Re denotes the relative size of the viscous force and the inertial force in the fluid motion, and We denotes the relative size of the internal action and the surface tension, which can only be obtained if the velocity is known.[16]

3. Initial conditions

The geometric model of this research is shown in Fig. 1. The gas phase is a pair of coaxial air bubbles of equal radius, and the liquid phase is water. The gas phase to the liquid phase has a density ratio of 1 : 1000, a viscosity ratio of 1 : 100,[17] and a relative magnetic permeability ratio of 1 : 1.5. It is assumed that both the gas phase and the liquid phase are both viscous and incompressible and the initial shape of the bubbles is a sphere. The initial distance between the centers of the two bubbles is three times the radius of the bubble. In order to eliminate the influence of the geometric wall on the bubble dynamics, the initial distance between the center of the bubble and the vertical wall is four times the radius of the bubble.[9]

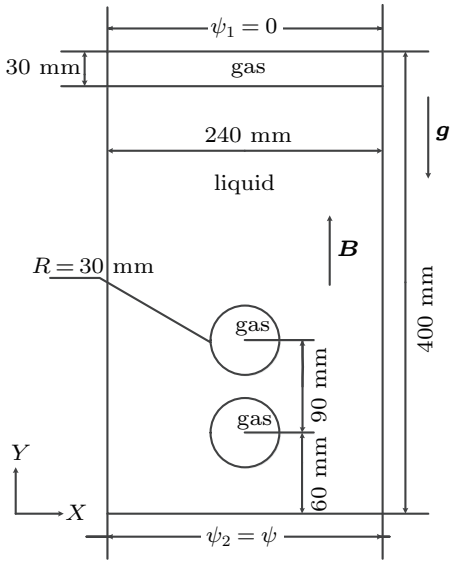


Fig. 1. Schematic diagram of the two-dimensional geometric model.

In order to fully observe the terminal velocity and final shape of the bubble, the vertical height should be set to be large enough, it is larger than 10 times the bubble radius, which was set to 400 mm in this study. The initial velocity of the bubbles is 0 m/s. We set the magnetic scalar potential at the top of the model to 0 A and the magnetic scalar potential at the bottom of the model to ψ. A vertically uniform magnetic field was formed inside the model.

4. Results and discussion

4.1. Verification of model accuracy and reliability

The interface information functions in the VOF and level-set methods are the volume ratio of the fluid independent of the flow parameters and the signed distance function of the interface, respectively. And the phase variables in the phase field method are the physical quantities associated with the flow parameters. In this case, the CH equation can be solved by coupling with the flow control equation, thereby avoiding the destruction of the physical conservation relationship caused by artificial processing near the interface.

Figure 2 shows the bubble mass per unit volume changing with time. It can be seen from the figure that the whole curve is relatively flat. The loss of bubble mass is less than 1% in the whole bubble movement process, which indicates the conservation of bubble mass in the simulation process, and also proves the reliability and accuracy of the model.

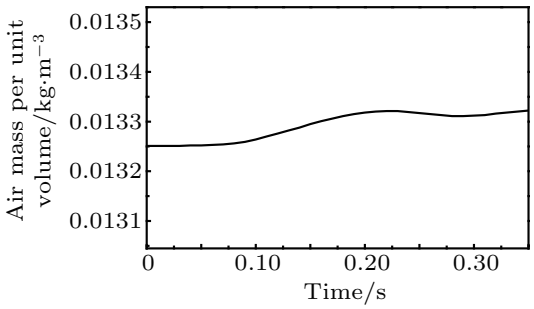


Fig. 2. Air mass per unit volume as a function of time.

In Fig. 3, the calculation results of this investigation are compared with the results of Hadidi *et al.*[12] The compared results show that our calculations are basically consistent with theirs, and the reliability and accuracy of the model are proved again.

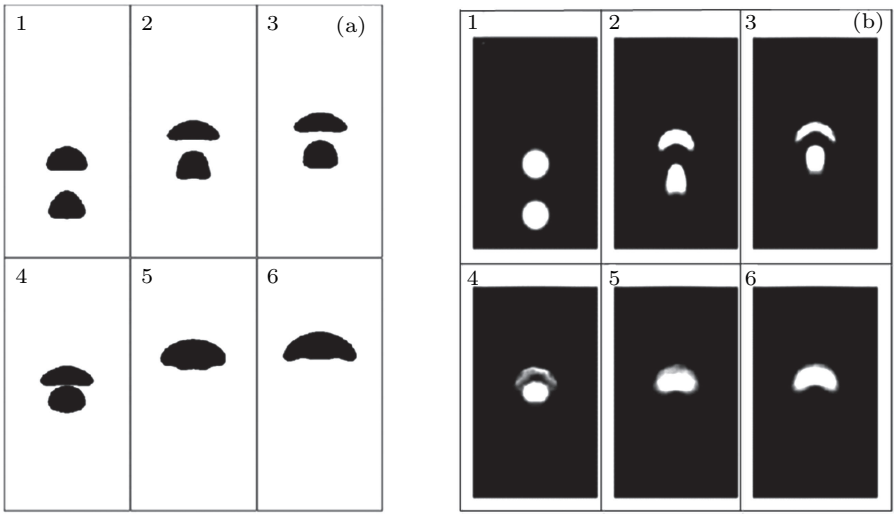


Fig. 3. Comparison between the results obtained in this study and those obtained in the literature: (a) the numerical results of Hadidi *et al.*[12] using the level-set method; (b) numerical results of this study.

4.2. Coaxial coalescence of a pair of bubbles under a uniform magnetic field

Figures 4(a) and 4(b) are the comparisons of the rise of a pair of coaxial bubbles on the vertical line under the effects of a uniform magnetic field without a magnetic field ($\psi = 0$ A) and $\psi = 1.5 \times 10^4$ A, respectively. As can be seen from Fig. 4(a), due to the wake effect of the leading bubble, a low pressure region is formed behind it, causing trailing bubbles to be drawn into the region. Because the attraction of the leading bubble to the trailing bubble causes the trailing bubble becoming a pear-like shape. As the suction and the resistance acting on the trailing bubble decrease, the velocity of rise of the trailing bubble increases. This effect causes the trailing bubble to rise faster than the leading bubble and bring them closer to each other, finally causing the trailing bubble to reach the leading bubble and be coalesced into it.[21] Figure 4(b) shows the effect of the dynamics and geometrical deformation of a pair of coaxial vertically rising bubbles under an applied uniform magnetic field of $\psi = 1.5 \times 10^4$ A. It can be seen that the shape of the trailing bubble changes in comparison to the case without a magnetic field. At $t = 0.06$ s, the elliptic bubbles in Fig. 4(b) are longer in the vertical direction and narrower in the horizontal direction than those in Fig. 4(a). The more obvious geometric deformation is observed at $t = 0.10$ s.

In Fig. 4(a), the trailing bubble is pear-shaped, while in figure 4(b), it is elliptic with narrow ends and wide middle. At the same time, the distance between leading bubbles and trailing bubbles becomes shorter. When $t = 0.15$ s, it can be seen that the distance between leading bubbles and trailing bubbles becomes shorter under the applied uniform magnetic field of $\psi = 1.5 \times 10^4$ A compared with that without magnetic field. At $t = 0.20$ s, without magnetic field, the leading bubbles and trailing bubbles have not coalesced, while the leading bubbles and trailing bubbles have begun to coalesce under the applied uniform magnetic field of $\psi = 1.5 \times 10^4$ A. It can be seen that the applied uniform magnetic field can affect the dynamics and geometric deformation of a pair of coaxial vertical rising bubbles in this model.

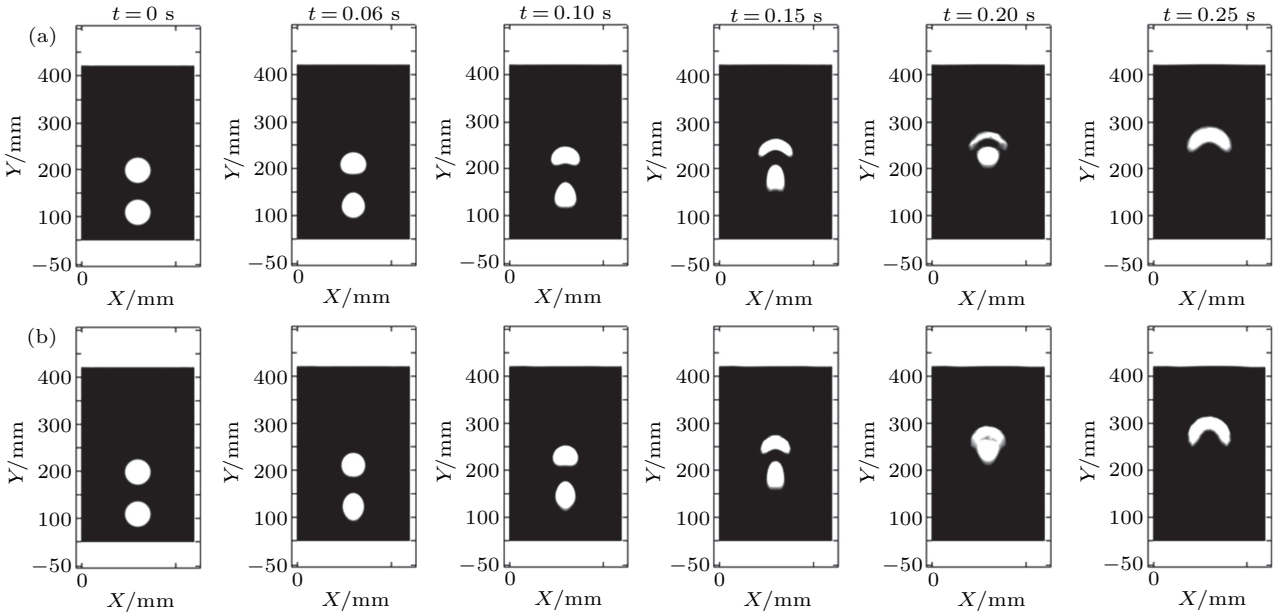


Fig. 4. The influence of magnetic field and no magnetic field on the rise and interaction of a pair of bubbles at different times: (a) $\psi = 0$ A; (b) $\psi = 1.5 \times 10^4$ A.

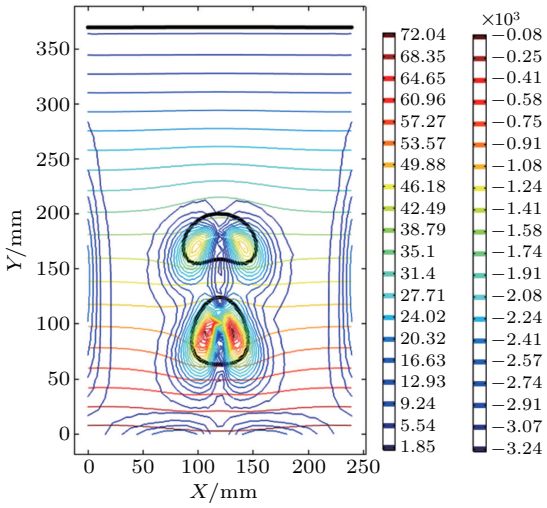


Fig. 5. Eddy current size and pressure distribution without magnetic field.

Figure 5 shows the contour of the vortex size and pressure without the magnetic field at $t = 0.1$ s. The first column of the right color ruler is the vortex size (in units of 1/s), the second column is the pressure (in units of Pa). It can be seen that vortexes form on the lower side of both sides of leading bubbles, while the vortexes near the coaxial vertical line following the bubbles and leading bubbles are quite sparse. Because of the influence of the surface tension, the pressure distribution in the bubble is larger than that of the external liquid. There is a low pressure zone which is formed at the bottom of the leading bubble, and it causes a suction effect on the trailing bubble. Due to this suction and reduction in drag force acting on the trailing bubble, the rising velocity of the trailing bubble is increased and will be larger than that of the leading bubble.[14] This explains why the trailing bubbles are attracted by the leading bubbles and gradually become a pear-like shape.

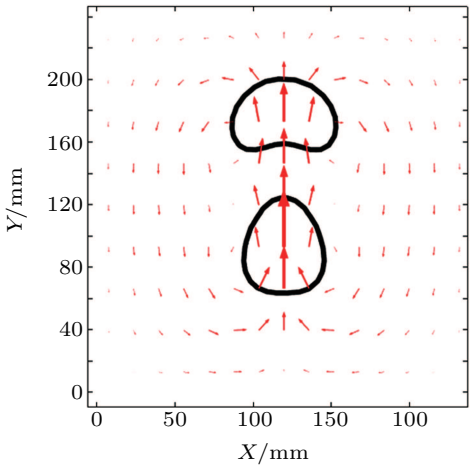


Fig. 6. The velocity vector at $t = 0.1$ s.

In order to more clearly observe the direction and magnitude of the velocity around the rising bubble, figure 6 is an

enlarged view of the velocity vector without a magnetic field at $t = 0.1$ s. Where the direction of the arrow is the direction of the velocity and the length of the arrow is the magnitude of the velocity. It can be seen that the entire flow field is relatively dense and symmetrical along the central axis, on which the velocity direction is vertically upward and the velocity is the largest. The internal velocity direction of the bubble is upward, while the outer velocity direction of the bubble is mostly downward. At the end of the bubble there is a backflow zone which is similar to a magnetic field line coming out of a magnet, coming out from the top and coming back from the bottom. The reason is that the density of the bubbles is less than the density of the surrounding liquid. The bubble rises from the bottom under the action of buoyancy, gravity, *etc*. and affects the movement of the surrounding liquid.

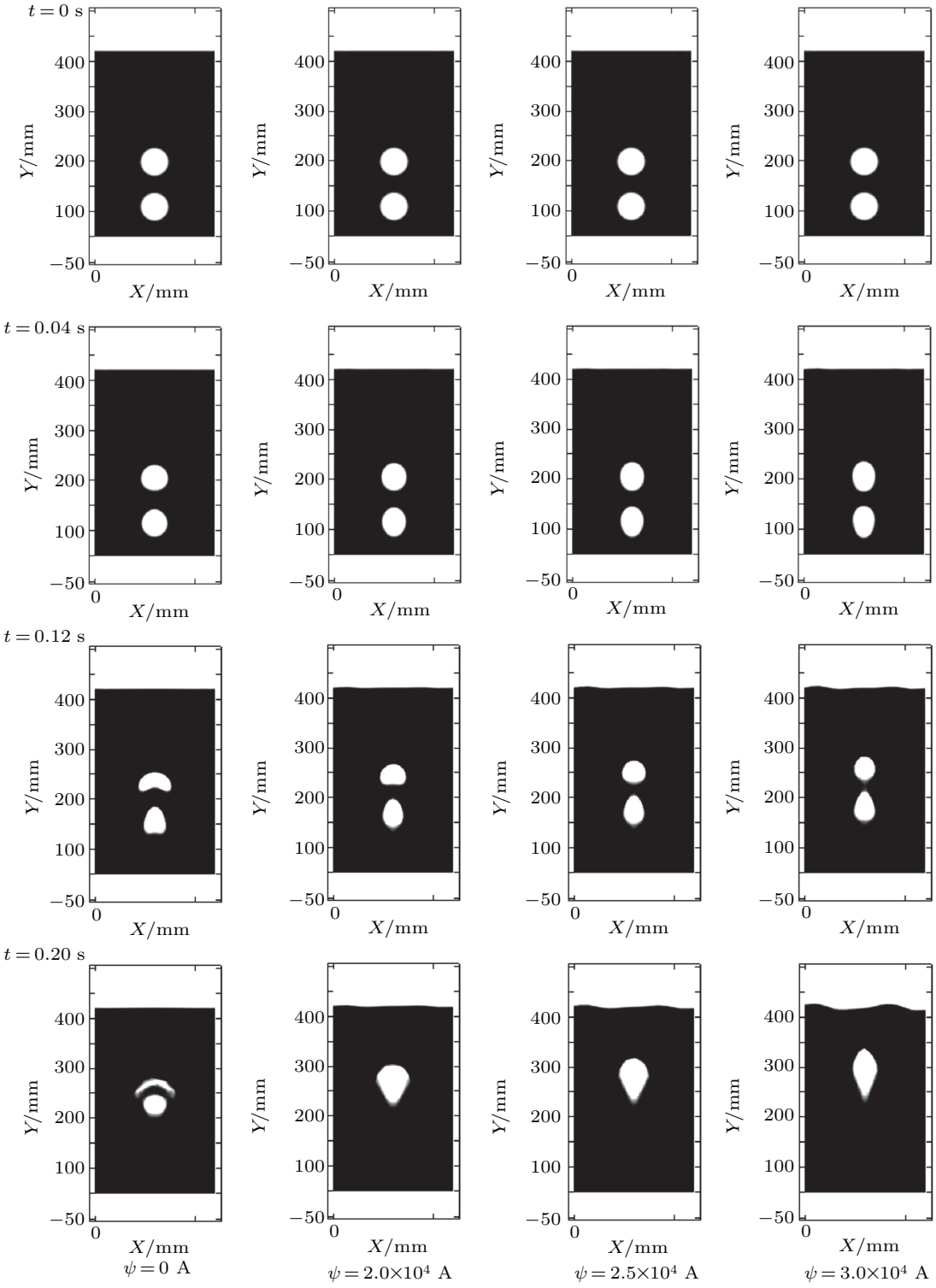


Fig. 7. The interaction of a pair of rising bubbles with multiple magnetic fields of different intensities at different time.

Different applied magnetic field intensities have different effects on the dynamics and geometric deformation of a pair of coaxial vertical rising bubbles. Figure 7 shows the effect of a uniform magnetic field at different intensities on the dynamics and geometrical deformation of a pair of coaxial vertically rising bubbles. The first column on the right is the case of no magnetic field, and the following three columns are the cases of the magnetic scalar potential at 2.0×10^4 A, 2.5×10^4 A, 3.0×10^4 A, respectively. It can be seen that as the magnetic field intensity increases, the bubbles become narrower in the horizontal direction and longer in the vertical direction. As the bubbles become narrower, the cross-sectional area of the bubbles becomes smaller, reducing the resistance received when the bubbles rise, thus increasing the rising velocity of the bubbles. Meanwhile, since the bubbles become longer, the vertical distance between leading bubbles and trailing bubbles becomes shorter, which accelerates the coalescence of bubbles. At $t = 0.04$ s, as the magnetic field intensity increases, the vertical distance between the leading bubbles and trailing bubbles in each column is smaller than in the previous column. At $t = 0.20$ s, as the magnetic field intensity increases, the top of the bubble in each column reaches a higher height than the top of the bubble in the previous column. Reaching higher heights in the same time means that the bubbles in each column rise faster than those in the previous column.

The applied uniform magnetic field can effectively shorten the distance between leading bubbles and trailing bubbles. Figure 8 shows the effect of uniform magnetic field on the distance between bubbles under three different magnetic scalar potentials. It can be seen that in a uniform magnetic field, the distance between bubbles rising at the same time is smaller than that in a non-magnetic field. As the intensity of uniform magnetic field increases, the distance between bubbles decreases: the larger the intensity of the uniform magnetic field, the smaller the distance between bubbles. It indicates that the applied uniform magnetic field can effectively shorten the vertical distance between the leading bubbles and the trailing bubbles.

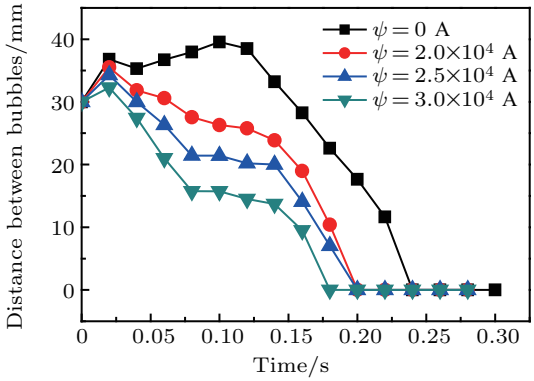


Fig. 8. Time-dependent bubbles distance under different uniform magnetic fields.

An applied uniform magnetic field can effectively shorten the time of coalescence of leading bubbles and trailing bubbles. Figure 9 shows the time curve of a pair of coaxial vertical rising bubbles coalescing. It can be seen that the time of the coalescence decreases from 0.22 s to 0.18 s, and the curve in the interval from $\psi = 2.0\times10^4$ A to $\psi = 3.0\times10^4$ A approximates a straight line with a downward trend. It indicates that with the increase of magnetic field intensity, the time of coalescence of a pair of vertical coaxial bubbles decreases and is inversely proportional to the magnetic field intensity in a certain range.

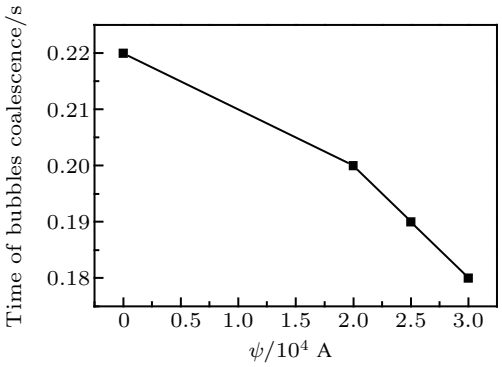


Fig. 9. Time of bubble coalescence under different magnetic fields.

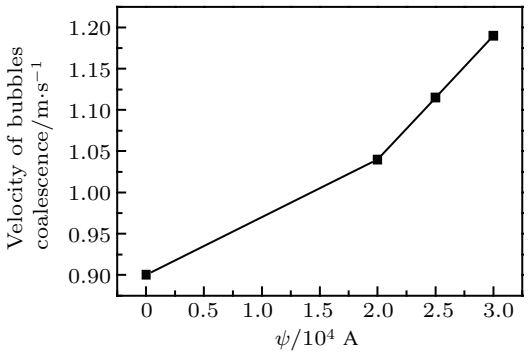


Fig. 10. The velocity of bubbles coalescence under different magnetic fields.

The applied uniform magnetic field can effectively increase the velocity of bubbles coalescence. Figure 10 shows the curve of the velocity when a pair of coaxial vertically rising bubbles coalesce and the average velocity when bubbles coalesce is selected here. The velocity of bubbles increases from 0.9 m/s to 1.19 m/s, and the curve between $\psi = 2.0\times10^4$ A and $\psi = 3.0\times10^4$ A is approximately a straight line with an upward trend. It indicates that with the increase of magnetic field intensity, the velocity of a pair of vertically rising coaxial air bubbles coalescing shows an upward trend and is proportional to the magnetic field intensity within a certain range.

According to the Faraday field line tube method in electromagnetic field, at the interface between the two media, as long as the permeability is not equal, the magnetic field force at the interface must be perpendicular to the interface, and always points from the medium with high permeability to the

medium with low permeability.[22] Figure 11 shows the distribution of relative permeability in this model. It can be clearly seen that the relative magnetic permeability inside the bubble is 1, while that of the liquid is 1.5, and that at the gas–liquid interface is between 1 and 1.5. From the surface of the bubble to the inside of the bubble, the relative magnetic permeability is constantly decreasing. According to the Faraday magnetic field tube method in the electromagnetic field, the magnetic field force should be perpendicular to the bubble surface and directed to the inside of the bubble.

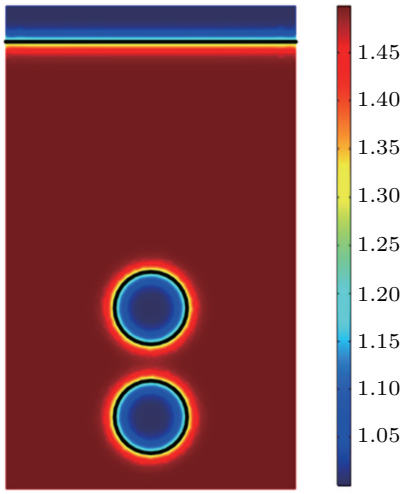


Fig. 11. Relative permeability distribution.

In Fig. 12, it can be seen that the magnetic field lines in the bubbles are more sparse than those in the surrounding fluid, indicating that the concentration of the magnetic field lines in the bubbles is smaller than that of the surrounding fluid. This is because the relative magnetic permeability of the gas phase is less than the relative magnetic permeability of the liquid phase, as shown in Fig. 11. Materials with high relative permeability will produce lower resistance when the magnetic field passes through, while those with low relative permeability will produce higher resistance when the magnetic field passes through, and magnetic field lines will be more inclined to pass through a region with low resistance.[12] Therefore, the concentration of the magnetic field lines in the bubbles is smaller than that of the surrounding fluid. The concentration of the magnetic field lines represents the intensity of the magnetic field, so a magnetic field gradient is generated at the interface of the two phases. Since the concentration of the magnetic field lines in the bubbles is smaller than that of the surrounding fluid, the direction of the magnetic field gradient is directed to the outside of the bubbles. The magnetic field gradient produces a magnetic force. Because the magnetic field gradient acts only at the interface of the two phases and the direction of the magnetic force is opposite to that of the magnetic field gradient, so the magnetic force acts only at the interface of the two phases and points to the inside of the bubbles. The arc diagram in the figure shows the magnetic field force at that point, and the unit of the color ruler is $\mathrm{N/m^3}$. The value of the magnetic field force at this point is a negative number, indicating that its direction is directed to the inside of the bubble. This result confirms our analysis. In Fig. 12, it can be seen that the concentration difference of the magnetic field lines on both sides in the horizontal direction from the center of the leading bubble to the end of the trailing bubble is the largest, so the force mainly squeezes the bubbles from both sides, causing the bubbles to become narrower and longer.

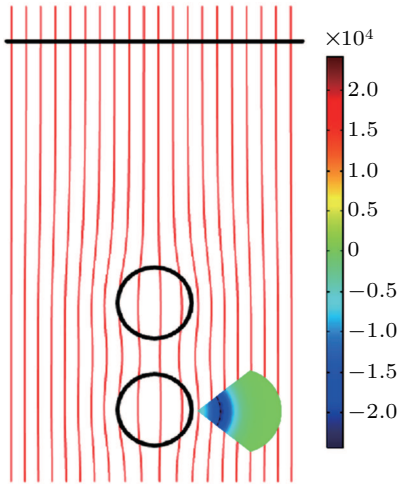


Fig. 12. Magnetic field lines and magnetic field forces.

Figure 13 shows a comparison of the volumetric force received by the bubbles at $t = 0$ s without a magnetic field and with the applied uniform magnetic field. The direction of the arrow represents the direction of the force, and the length of the arrow represents the magnitude of the force. It can be seen that when there is no applied magnetic field, the volumetric force received by the bubbles is substantially vertically downward, it is mainly gravity here. When the magnetic field is applied, the volumetric force on the bubble starts to point to the inside of the bubble. The volumetric force here is not perpendicular to the interface, because the volumetric force on the bubble is not only the magnetic field force, but mainly the combined force of magnetic field and gravity. It can be seen at the bottom of the bubbles that the direction of the magnetic field force here is vertically upward because it is perpendicular to the interface. However, since the direction of the magnetic force is opposite to the direction of the gravity, the length of the arrow here is very short, indicating that the volumetric force received by the bubbles is particularly small. The direction of the magnetic force on both sides of the bubble and the two horizontal points at the center of the bubble is horizontal and pointing to the center of the bubble. The direction of the magnetic force is vertical to the gravity, so the direction of the resultant force is inclined downward. The length of the arrow at this point is the longest, indicating that the volumetric force received there is the largest, as explained at the end

of the previous paragraph. It is the magnetic force generated by the applied uniform magnetic field that makes the bubbles to become narrower and longer. The narrowing of the bubbles causes the cross-sectional area of the bubbles to become smaller. As the cross-sectional area of the bubbles becomes smaller and smaller, the bubbles begin to become sharper and sharper. Due to the shape effect, the resistance of the bubbles is getting smaller and smaller, plus the suction effect, thereby increasing the velocity of the bubbles rising. The lengthening of the bubble causes the vertical distance between the leading bubble and the trailing bubble to be shortened, thereby accelerating the coalescence of the bubbles.

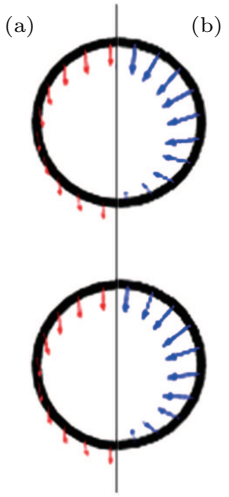


Fig. 13. Comparison of volumetric forces: (a) in the absence of magnetic field; (b) in an applied uniform magnetic field.

5. Conclusions

The interaction and coalescence of bubbles in a gas–liquid two-phase flow can have a significant effect on heat transfer, mass transfer, and chemical reactions in a gas–liquid system. In this study, a two-dimensional multi-field coupling model for simulating a pair of bubble rises in a gas–liquid two-phase flow is established by coupling the magnetic field, laminar flow, and phase field for the interaction and coalescence of bubbles in a gas–liquid two-phase flow. The geometric deformation and dynamic behavior of a pair of coaxial vertically rising bubbles in a uniform magnetic field in the vertical direction were investigated. The results show that the uniform magnetic field in the vertical direction will affect the shape of bubbles, making them narrower and longer, and the vertical distance between leading bubbles and trailing bubbles will also decrease. In the case of the magnetic scalar potential ranging from 2.0×10^4 A to 3.0×10^4 A, with the increase of the applied uniform magnetic field intensity, the velocity when a pair of coaxial vertically rising bubbles coalescence is proportional to the magnetic field intensity, and the time of coalescence is inversely proportional to the magnetic field intensity. This provides a way to effectively control the bubble change in the gas–liquid two-phase flow without contact and to a certain extent to ensure the personal safety of the experimental personnel and staff.

References

[1] Zhang C, Eckert S and Gerbeth G 2005 *Int. J. Multiphase Flow* **31** 824
[2] Liu J, Zhang H B 2019 *Acta Phys. Sin.* **68** 059401 (in Chinese)
[3] Li Y N, Hai M M, Zhao Y, Lv Y L, He Y, Ghen G, Liu L Y, Liu R C and Zhang G 2018 *Chin. Phys. B* **27** 128703
[4] Zhao N and Wang D H 2016 *Numerical Simulation of Multi-medium Fluid Interface Problems* (Beijing: Science Press) pp. 95–96 (in Chinese)
[5] Nakatsuka K, Jeyadevan B, Akagami Y, Torigoe T and Asari S 1999 *J. Magn. Magn. Mater.* **201** 256
[6] Tagawa T 2006 *Math. Comput. Simul.* **72** 212
[7] Ki 2010 *Comput. Phys. Commun.* **181** 999
[8] Shafiei Dizaji A, Mohammadpourfard M and Aminfar H 2018 *J. Magn. Magn. Mater.* **449** 185
[9] Ansari M R, Hadidi A and Nimvari M E 2012 *J. Magn. Magn. Mater.* **324** 4094
[10] Guo K K, Li H X, Feng Y, Wang T and Zhao J F 2019 *Int. J. Heat Mass Transfer* **134** 17
[11] Tian X H 2015 *Numerical Simulation of Bubble Motions in Conducting Fluid under Uniform-Vertical Magnetic Fields* (MS dissertation) (Chongqing: Chongqing University) (in Chinese)
[12] Hadidi A and Jalali-Vahid D 2016 *Theor. Comput. Fluid Dyn.* **30** 165
[13] Yue P, Feng J J, Liu C and Shen J 2004 *J. Fluid Mech.* **515** 293
[14] Zhu C S, Han D, Feng L and Xu S 2019 *Chin. Phys. B* **28** 034701
[15] Chiu P 2019 *J. Comput. Phys.* **392** 115
[16] Shen J and Yang X F 2010 *Chin. Ann. Math. Series B* **31** 743
[17] Zhu C S, Han D and Xu S 2018 *Chin. Phys. B* **27** 094704
[18] Liu J, Tan S H, Yap Y F, Ng M Y and Nguyen N T 2011 *Microfluid. Nanofluid.* **11** 177
[19] Gu X A, Xu Q X, Shen R Y and Xu J T 2002 *Noise Vibration Control* **4** 10 (in Chinese)
[20] Qin L, Tao L and Mo Y 2018 *Acta Phys. Sin.* **67** 234701 (in Chinese)
[21] Cheng M, Hua J S and Lou J 2010 *Comput. Fluids* **39** 260
[22] Yan W L, Yang Q X and Wang Y H 2005 *Numerical Analysis of Electromagnetic Fields in Electrical Engineering* (Beijing: Mechanical Industry Press) pp. 214–236 (in Chinese)